

# Chirped amplitude mode in photo-excited superconductors

Thomas Blommel,<sup>1</sup> Jason Kaye,<sup>2,3</sup> Yuta Murakami,<sup>4</sup> Emanuel Gull,<sup>1</sup> and Denis Golež<sup>5,6</sup>

<sup>1</sup>*Department of Physics, University of Michigan, Michigan, USA*

<sup>2</sup>*Center for Computational Quantum Physics, Flatiron Institute, 162 5th Avenue, New York, NY 10010, USA*

<sup>3</sup>*Center for Computational Mathematics, Flatiron Institute, 162 5th Avenue, New York, NY 10010, USA*

<sup>4</sup>*Center for Emergent Matter Science, RIKEN, Wako, Saitama 351-0198, Japan*

<sup>5</sup>*Jožef Stefan Institute, SI-1000, Ljubljana, Slovenia*

<sup>6</sup>*Faculty of Mathematics and Physics, University of Ljubljana, 1000 Ljubljana, Slovenia*

(Dated: March 5, 2024)

We show that the amplitude mode in superconductors exhibits chirped oscillations under resonant excitation and that the chirping velocity increases as we approach the critical excitation strength. The chirped amplitude mode enables us to determine the local modification of the effective potential even when the system is in a long-lived pre-thermal state. We then show that this chirped amplitude mode is an experimentally observable quantity since the photo-induced (super)-current in pump-probe experiments serves as an efficient proxy for the dynamics of the order parameter, including the chirped dynamics. Our result is based on the attractive Hubbard model using dynamical mean-field theory within the symmetry-broken state after a resonant excitation across the superconducting gap. Since the collective response takes place on emergently long timescales, we extend the hierarchical low-rank compression method for nonequilibrium Green's functions to symmetry-broken states and show that it serves as an efficient representation despite long-lived memory kernels.

*Introduction*— Soon after the seminal paper on BCS superconductivity [1], Anderson pointed out that the electromagnetic response of a superconductor leads to a collective response [2–4]. This realization had a profound impact on condensed matter physics, as well as particle physics, with the prediction of the Higgs mode [5, 6]. It took almost two decades before such an excitation was observed in 2H-NbSe<sub>2</sub> with the coexistence of superconductor and charge-density-wave [7–10] phases, and another three decades for direct observation using terahertz spectroscopy either in a pump-probe setup [11] or with third-harmonics generation [12, 13].

This progress opened the field of Higgs spectroscopy, which has now been applied to numerous superconducting materials, including superconductors with running supercurrents [14, 15] and unconventional superconductors [16, 17]. Ever more precise measurements of collective mode response enables the study of their long-time behavior after excitation both in solids [11] as well as quantum simulators [18–20].

The theoretical description of the the time evolution of the Higgs mode is difficult. Time-dependent Landau-Ginzburg theory assumes an ad-hoc rapid modification of the effective potential and damping is considered on the phenomenological level [21, 22]. Microscopic time-dependent BCS theory predicts richer dynamics, including a power-law decay [23, 24] or solitonic solution [25–27]. However, all these theoretical statements assume dissipationless electronic dynamics, which is questionable in real materials and opens up a question on the decay of collective modes upon the inclusion of electronic scattering.

The main difficulty of the theoretical description of electronic scattering on collective mode dynamics stems from the fact that collective response takes place on emer-

gently long time scales. This has limited previous studies to dissipationless dynamics [23–27], or when fluctuations were included, the description was limited to relatively short times with few coherent oscillations and limited information about amplitude mode lifetime [28–31].

Only recently, progress in numerical solvers for nonequilibrium Green's functions [32], including the generalized Kadanoff-Baym ansatz [33–36] and memory kernel truncation methods [37, 38], has allowed access to long enough times to examine these questions. However, the application of these techniques to symmetry-broken phases is much less understood due to the long-lived power-law correlators acting as memory kernels.

In this work, we study the long-time evolution of collective modes by solving the full Kadanoff-Baym equations (KBE), and show that the order parameter displays an extremely slow approach to a thermal state. Within such a nonthermal state, the amplitude mode exhibits chirping (dynamical decrease in the frequency). The velocity of the chirping increases as we approach the nonthermal critical excitation strength at which the order parameter vanishes in the long time limit. We show that the effect is experimentally accessible in tera-hertz pump-probe experiments by directly measuring the probe-induced currents, which can be used to extract the dynamics of the order parameter with a small imprint of the quasiparticle response.

We also highlight our use of the hierarchical off-diagonal low-rank (HODLR) compression method for the numerical solution of the KBE [39]. The standard  $\mathcal{O}(N^3)$  scaling of the direct solution of the KBE with the number of time steps  $N$ , resulting from memory terms, typically prevents access to the time scales necessary to analyze the lifetime of collective excitations [28–30, 32]. A new class of data compression-based meth-

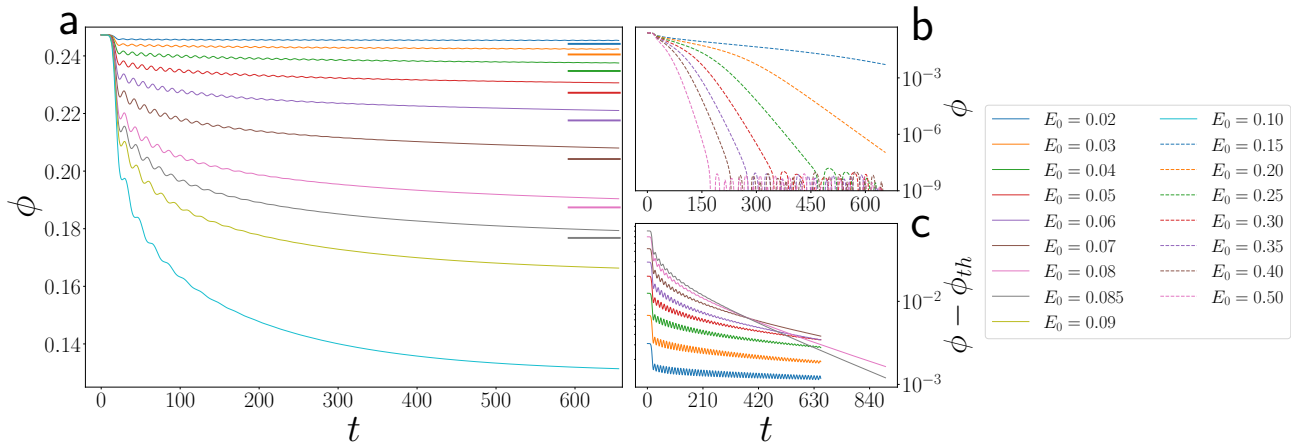


FIG. 1. Time evolution of the order parameter  $\phi$  after photoexcitation with pump amplitude  $E_0$  in the (a) weak excitation regime  $E_0 < E_{0c}$ , in which amplitude mode oscillations are present, and (b) the strong excitation regime  $E_0 \geq E_{0c}$ , in which we observe superexponential decay. The noise at small values in (b) is consistent with the truncation tolerance  $10^{-8}$  used in the HODLR compression scheme. (c) The system exponentially approaches the expected thermal values (thick bars on right-hand side of (a)).  $E_0 = 0.08, 0.085$  are integrated further in time to emphasize the exponential decay.

ods, including the HODLR approach, have recently been proposed to overcome this bottleneck [40–44]. Viewing two-time Green’s functions as matrices, the HODLR method decomposes these matrices into blocks, refined towards the diagonal, which in many cases have been observed to be numerically low-rank. A truncated singular value decomposition of these blocks is systematically updated on-the-fly during time-stepping and used to compute history integrals with controllable accuracy, yielding an  $\mathcal{O}(k^2 N^2 \log N)$  computational complexity and  $\mathcal{O}(kN \log N)$  memory complexity, for  $k$  the maximum block rank, without modifying the underlying KBE. Using this method, we demonstrate a 100-fold decrease in the computational cost required to propagate to the time scales studied compared with direct time stepping, with 50–200 times less memory.

*Model and method*– We study superconductivity within the attractive Hubbard model

$$H = -t_0 \sum_{\langle j,k \rangle \sigma} e^{iqA(t)} d_{j\sigma}^\dagger d_{k\sigma} - U \sum_j (n_{j\uparrow} - 1/2)(n_{j\downarrow} - 1/2), \quad (1)$$

where  $d_{i\sigma}$  is the annihilation operator at site  $i$  and spin  $\sigma$ ,  $n_{i\sigma}$  is the spin-dependent density operator and  $q$  is the charge. We set the energy to the hopping amplitude  $t_0 = 1$ , the Coulomb attraction to  $U = 2$ , and fix the occupation at half filling.

We solve the problem within time-dependent dynamical mean-field theory (DMFT) on the Bethe lattice and explicitly break the superconducting symmetry. This leads to matrix-valued Green’s functions  $G_{\alpha\beta}(t, t') = -i\langle \mathcal{T} \psi_\alpha(t) \psi_\beta^\dagger(t') \rangle$ , with the Nambu spinor  $\psi = \{d_\uparrow, d_\downarrow^\dagger\}$ . For the impurity solver, we use the self-consistent second-order perturbation theory known as second Born, or GF2 [45–47]. Collective order parameter dynamics take place on long time scales, and such long-time integration

of the KBE is made possible by using a compressed representation of the Green’s function to reduce both the computational and memory complexity [39]. We refer to the appendices for further implementation details.

We induce a dynamical perturbation by a short pump pulse introduced by a Peierls substitution in Eq. 1. The electric field  $E_p = -\partial_t A$  is parameterized as

$$E_P(t) = E_0 \exp\left(-\frac{(t-t_c)^2}{\sigma^2}\right) \sin(\omega(t-t_c)), \quad (2)$$

with pulse center  $t_c$ , pulse width  $\sigma$ , driving frequency  $\omega$ , and amplitude  $E_0$ .

*Results*– For an interaction strength of  $U = 2$  the attractive Hubbard model in equilibrium has a phase transition at inverse temperature  $1/T_c = \beta_c \approx 10.6$  within the GF2 approximation. Across this transition, the system develops a nonzero superconducting order parameter  $\phi(t) = \sum_k \langle c_{k\downarrow} c_{-k\uparrow} \rangle$ . We choose a temperature  $\beta = 18$  deep in the ordered state, and find that the system has a band gap of  $\Delta \approx 0.65$ .

To excite the amplitude mode, we pump the system with a pulse tuned to twice the band gap ( $t_c = 16$ ,  $\sigma = 6.5$ ,  $\omega = 2\Delta$ ). The time evolution of the order parameter is presented in Fig. 1. At weak excitation strength, the order parameter decays at an extremely slow exponential rate [48, 49]. The expected thermal states, marked by the horizontal lines, are not reached on the time scale of our simulation; see also Fig. 1(c), in which the thermal values are subtracted. For intermediate pump strengths, we observe the decay of the order parameter through several orders of magnitude. On top of the exponential relaxation, well-defined oscillations correspond to the amplitude mode excitation [10, 50]. As the pump strength is increased, the initial amplitude of these oscillations increases; however, they also have

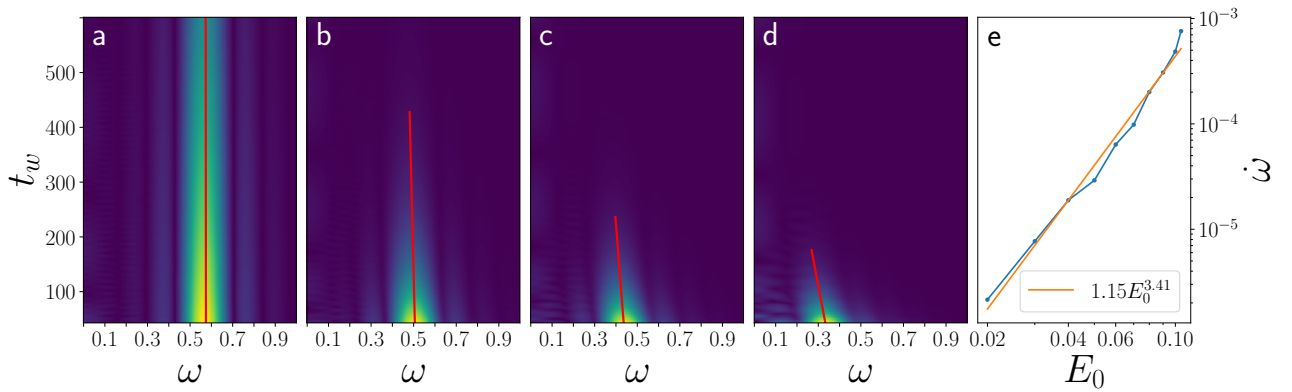


FIG. 2. (a-d): Windowed Fourier transform  $F[\phi](t_w)$  of the order parameter centered around  $t_w$  with exponential background subtracted, for pump amplitudes  $E_0 = 0.02, 0.06, 0.08,$  and  $0.1$ . The red line is a linear fit to the maximum. (e) Slope of the maxima (chirping velocity), shown by red lines, for different pump intensities (blue) with the best fit (orange).

shorter lifetimes. Increasing the pump amplitude further, we reach a critical point at which these oscillations disappear. In this regime, the order parameter goes to zero in the long-time limit, see Fig. 1(b), and transiently critical behaviour of the order parameter takes place [48, 51, 52].

We observe that the frequency of the collective mode oscillations gradually chirps to smaller values. To extract the chirping velocity, we first subtract the background exponential decay from the data in Fig. 1, and then compute a windowed Fourier transform  $\text{FT}[\phi](t_w) = \int_0^{T_{max}} dt \phi(t) e^{-i\omega t - (t-t_w)^6/\sigma_w^6}$ . We define the chirping velocity  $\dot{\omega}$  as the slope of the maximum of  $\text{FT}[\phi](t_w)$ , which is tracked in Fig. 2(a-d) for increasing pump amplitudes. Fig. 2(e) shows that the chirping velocity follows a power-law scaling  $\dot{\omega} \propto E_0^{3.41}$  with the pump amplitude, slightly faster than the scaling  $j \propto E_0^3$  of the current due to photo-induced amplitude mode oscillations [24, 50].

Whereas the dissipationless BCS dynamics lead to power-law decay of the oscillation amplitude [23], the description based on the attractive Hubbard model includes fluctuations, and exhibits exponential decay. This is consistent with the effect of thermal noise on the dissipationless BCS dynamics [25, 53]. The lifetime of the amplitude mode decays with increasing pump strength (see Fig. 2(a-d)), and changes by more than an order of magnitude from the weak to the strong excitation regime.

The chirping of the amplitude mode is the main result of this work. We emphasize that observing such phenomena requires microscopic treatment of fluctuations beyond the mean-field theory, in a full nonequilibrium setup, as the resulting state is highly nonthermal. Moreover, the chirping phenomena is not limited to superconductors, but should be observed in any system with broken symmetry, like magnetic [54] or charge density waves [55, 56]. In actual experimental setups, there is a trade-off in pump strength between the chirping velocity and the lifetime of the amplitude mode, which depends on the details of the pulse and the material studied.

Now, we interpret the microscopic dynamics within the time-dependent Landau-Ginzburg theory. The chirping of the amplitude mode corresponds to a dynamical reduction of the local curvature due to the feedback of the electronic scattering on the collective order. While it would be tempting to interpret the chirping as a heating effect within the Landau-Ginzburg theory, we emphasize that the system is closed and in a prethermal regime, which the temperature change cannot describe. In principle, one could construct a time-dependent Landau-Ginzburg theory of chirping. However, it is difficult in practice to extract the evolution of global structure of the Landau-Ginzburg potential, even when microscopic dynamics are available. An important consequence of our analysis is that the chirped frequency can act as a microscopic measure of the dynamically modified local curvature.

We next discuss how this physics could be observed experimentally. The amplitude mode does not couple linearly to light; however, it can be observed in nonlinear processes, such as pump-probe setups [11] or the third-harmonics response [12, 24, 50]. Our numerical tests agree with previous observations that it is difficult to extract the amplitude mode signal from the optical response due to the overlap with the quasiparticle continuum [30]. However, we observe that the photo-induced current serves as an excellent proxy for the dynamics of the order parameter. While in principle the optical conductivity and photo-induced current carry similar information, we found that in practice it is much easier to extract coherent oscillations from the time-dependent current, compared with spectral analysis of the optical conductivity.

We evaluate the probe-induced current by directly simulating an additional probe pulse at a time  $\tau$  after the pump pulse, and measuring the induced current [57–59]. This approach is theoretically convenient as it includes vertex corrections to the response function, which represents the contribution from the collective modes [60, 61].

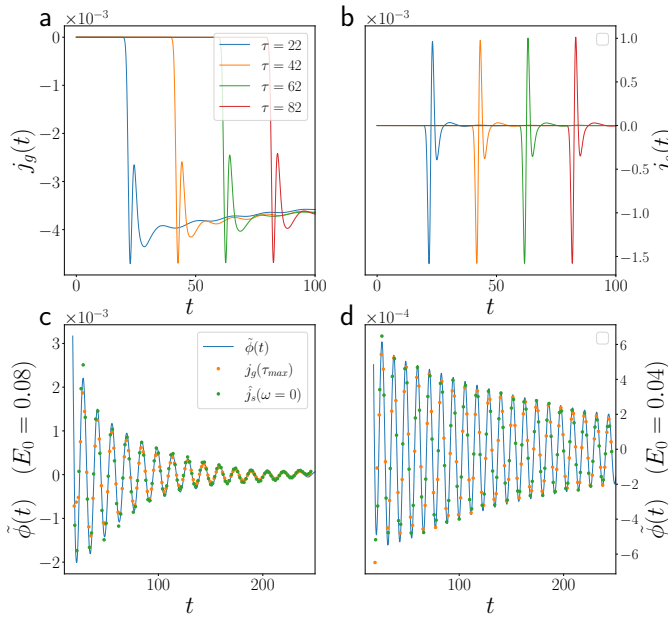


FIG. 3. Current induced by (a) Gaussian probe pulse  $j_g$  with parameters  $E_0 = 0.1E_0^{\text{Pump}}$ ,  $t_c = t_c^{\text{Pump}} + \tau$ ,  $\sigma = 1$ , and (b) monocycle probe pulse  $j_s$  with parameters  $E_0 = 0.1E_0^{\text{Pump}}$ ,  $t_c = t_c^{\text{Pump}} + \tau$ ,  $\sigma = 1$ ,  $\omega = 1$ . (c) Comparison of the order parameter oscillations with subtracted background  $\tilde{\phi}(t)$  with two separate quantities: the maximum current response  $\max(j_g)$  induced by Gaussian pulse, and the integral  $\hat{j}_s(\omega = 0)$  over the current, for pump amplitudes  $E_0 = 0.08$  (c) and  $E_0 = 0.04$  (d).

We propose two probe protocols and show that the current response in both cases could be connected with the collective dynamics of the amplitude mode. In the first setup, we model the probe as a small Gaussian pulse, with amplitude one-tenth that of the pump pulse. We measure the current response to the probe,  $j_g(t)$ , shown in Fig. 3(a), where each line corresponds to the same probe applied at different values of  $\tau$ . Figs. 3(c,d) show the first local minima versus the delay time  $\tau$ . We see that the current tracks the oscillations of the order parameter for both pump strengths considered, giving information about both the chirped frequency and the lifetime of the amplitude mode.

Since measuring the fast current response might be experimentally difficult, we show that the time-integrated current also tracks the order parameter. For this case, we focus on a monocycle pulse parameterized by Eq. 2, with parameters  $\sigma = 1$ ,  $t_c = 16 + \tau$ ,  $\omega = 1$ , and an amplitude one-tenth that of the pump pulse. Here, since the electric field integrates to zero, the current decays to zero after some time. Fig. 3(b) shows the current for this experimental setup. The green data points in Figs. 3(c,d) correspond to the integral of the current, and also closely track the order parameter.

Based on these results, we propose that the direct mea-

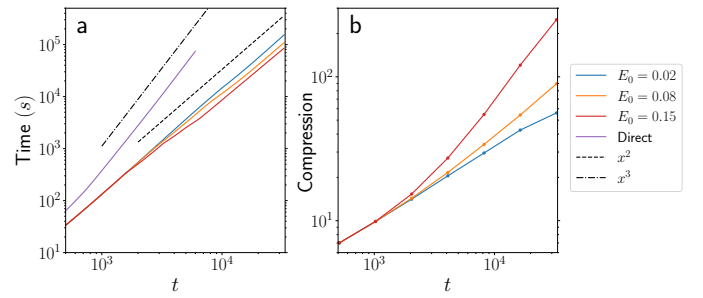


FIG. 4. (a) Wall clock time and (b) compression factor with increasing number of timesteps for HODLR propagation scheme versus direct time stepping, for various pump intensities  $I$  starting from the equilibrium state at  $\beta = 18$ .

surement of the photo-induced current is a convenient way to measure amplitude mode response. The photo-induced current and chirping can be measured in the pump-probe setup using either free-space electro-optic sampling, like in Ref. [11], or transmission line experiments, which were recently used to detect superconducting nonlinear transport [62], the light-induced anomalous quantum Hall effect due to circularly polarized light [63], and ultrafast resistive switching in 1T-TaS<sub>2</sub> [64].

Since our analysis was enabled by the HODLR compression technique for the numerical solution of the KBE [39], we consider the compressibility of the dynamics of symmetry-broken states, and the performance of the scheme compared with the direct solution of KBE. In Fig. 4(a), we observe approximately quadratic scaling of the computational cost with the propagation time over a range of pump intensities and equilibrium state temperatures. We reach 32000 time steps in roughly one day on a single-core of a workstation using 0.5 GB of memory. By contrast, we extrapolate that cubic-scaling direct time stepping using the NESSi code [32] would have taken 129 days with 137 GB of memory. Fig. 4(b) shows a factor 50-200 memory compression of the Green's function and self-energy compared with direct storage on a two-time grid. The Appendix considers the compressibility in more detail.

We have shown that the collective amplitude mode displays chirped dynamics after the above gap excitation, and have analyzed a direct experimental signature of the response based on the photo-induced current within the pump-probe setup. Future applications include the nonlinear response of unconventional superconductors [16, 17], and extensions beyond dynamical mean-field theory to study spatial fluctuations [65] and the build-up of the fluctuating order in systems with competing orders [66, 67]. Methodologically, this work represents the first application of the HODLR compression technique for the KBE to symmetry-broken states, and demonstrates that it can access long enough time scales for the practical study of a broad field of photo-induced

phase transitions [68–71].

DG acknowledges the support of the projects J1-2463, N1-0318, MN-0016-106, and P1-0044 program of the Slovenian Research Agency. TB was funded by the Department of Energy via Grant No. DE-SC0020347 until Aug. 2023. TB as of Aug. 2023 and EG were supported by the U.S. Department of Energy, Office of Science, Office of Advanced Scientific Computing Research and Office of Basic Energy Sciences, Scientific Discovery through Advanced Computing (SciDAC) program under Award Number(s) DE-SC0022088. YM is supported by Grant-in-Aid for Scientific Research from JSPS, KAKENHI Grant Nos. JP20K14412, JP21H05017 and JST CREST Grant No. JPMJCR1901. The Flatiron Institute is a division of the Simons Foundation.

- 
- [1] J. Bardeen, L. N. Cooper, and J. R. Schrieffer, *Phys. Rev.* **108**, 1175 (1957).
- [2] P. W. Anderson, *Phys. Rev.* **110**, 827 (1958).
- [3] P. W. Anderson, *Phys. Rev.* **112**, 1900 (1958).
- [4] P. W. Anderson, *Phys. Rev.* **130**, 439 (1963).
- [5] P. Higgs, *Physics Letters* **12**, 132–133 (1964).
- [6] P. W. Higgs, *Phys. Rev. Lett.* **13**, 508 (1964).
- [7] R. Sooryakumar and M. V. Klein, *Phys. Rev. Lett.* **45**, 660 (1980).
- [8] P. B. Littlewood and C. M. Varma, *Phys. Rev. Lett.* **47**, 811 (1981).
- [9] P. B. Littlewood and C. M. Varma, *Phys. Rev. B* **26**, 4883 (1982).
- [10] D. Pekker and C. Varma, *Annual Review of Condensed Matter Physics* **6**, 269 (2015), <https://doi.org/10.1146/annurev-conmatphys-031214-014350>.
- [11] R. Matsunaga, Y. I. Hamada, K. Makise, Y. Uzawa, H. Terai, Z. Wang, and R. Shimano, *Phys. Rev. Lett.* **111**, 057002 (2013).
- [12] R. Matsunaga, N. Tsuji, H. Fujita, A. Sugioka, K. Makise, Y. Uzawa, H. Terai, Z. Wang, H. Aoki, and R. Shimano, *Science* **345**, 1145 (2014).
- [13] R. Matsunaga, N. Tsuji, K. Makise, H. Terai, H. Aoki, and R. Shimano, *Phys. Rev. B* **96**, 020505 (2017).
- [14] A. Moor, A. F. Volkov, and K. B. Efetov, *Phys. Rev. Lett.* **118**, 047001 (2017).
- [15] S. Nakamura, Y. Iida, Y. Murotani, R. Matsunaga, H. Terai, and R. Shimano, *Phys. Rev. Lett.* **122**, 257001 (2019).
- [16] K. Katsumi, N. Tsuji, Y. I. Hamada, R. Matsunaga, J. Schneeloch, R. D. Zhong, G. D. Gu, H. Aoki, Y. Gallais, and R. Shimano, *Phys. Rev. Lett.* **120**, 117001 (2018).
- [17] H. Chu, M.-J. Kim, K. Katsumi, S. Kovalev, R. D. Dawson, L. Schwarz, N. Yoshikawa, G. Kim, D. Putzky, Z. Z. Li, *et al.*, *Nature communications* **11**, 1793 (2020).
- [18] D. J. Young, A. Chu, E. Y. Song, D. Barberena, D. Wellnitz, Z. Niu, V. M. Schäfer, R. J. Lewis-Swan, A. M. Rey, and J. K. Thompson, *Nature* **625**, 679–684 (2024).
- [19] R. J. Lewis-Swan, D. Barberena, J. R. K. Cline, D. J. Young, J. K. Thompson, and A. M. Rey, *Phys. Rev. Lett.* **126**, 173601 (2021).
- [20] A. Behrle, T. Harrison, J. Kombe, K. Gao, M. Link, J.-S. Bernier, C. Kollath, and M. Köhl, *Nature Physics* **14**, 781 (2018).
- [21] I. S. Aranson and L. Kramer, *Rev. Mod. Phys.* **74**, 99 (2002).
- [22] A. Zong, P. E. Dolgirev, A. Kogar, E. Ergeçen, M. B. Yilmaz, Y.-Q. Bie, T. Rohwer, I.-C. Tung, J. Straquadine, X. Wang, Y. Yang, X. Shen, R. Li, J. Yang, S. Park, M. C. Hoffmann, B. K. Ofori-Okai, M. E. Kozina, H. Wen, X. Wang, I. R. Fisher, P. Jarillo-Herrero, and N. Gedik, *Phys. Rev. Lett.* **123**, 097601 (2019).
- [23] A. F. Volkov and S. M. Kogan, *Zh. Eksp. Theor. Fiz.* **65**, 2038 (1973).
- [24] N. Tsuji and H. Aoki, *Phys. Rev. B* **92**, 064508 (2015).
- [25] R. A. Barankov, L. S. Levitov, and B. Z. Spivak, *Phys. Rev. Lett.* **93**, 160401 (2004).
- [26] E. A. Yuzbashyan, O. Tsypliyatyev, and B. L. Altshuler, *Phys. Rev. Lett.* **96**, 097005 (2006).
- [27] R. A. Barankov and L. S. Levitov, *Phys. Rev. Lett.* **96**, 230403 (2006).
- [28] A. F. Kemper, M. A. Sentef, B. Moritz, T. P. Devereaux, and J. K. Freericks, *Annalen der Physik* **529**, 1600235 (2017).
- [29] B. Nosarzewski, B. Moritz, J. K. Freericks, A. F. Kemper, and T. P. Devereaux, *Phys. Rev. B* **96**, 184518 (2017).
- [30] A. Kumar and A. F. Kemper, *Phys. Rev. B* **100**, 174515 (2019).
- [31] Y. Murakami, P. Werner, N. Tsuji, and H. Aoki, *Phys. Rev. B* **94**, 115126 (2016).
- [32] M. Schüler, D. Golež, Y. Murakami, N. Bittner, A. Herrmann, H. U. Strand, P. Werner, and M. Eckstein, *Computer Physics Communications* **257**, 107484 (2020).
- [33] P. Lipavský, V. Špička, and B. Velický, *Phys. Rev. B* **34**, 6933 (1986).
- [34] R. Tuovinen, D. Golež, M. Eckstein, and M. A. Sentef, *Phys. Rev. B* **102**, 115157 (2020).
- [35] N. Schlünzen, J.-P. Joost, F. Heidrich-Meisner, and M. Bonitz, *Phys. Rev. B* **95**, 165139 (2017).
- [36] Y. Pavlyukh, E. Perfetto, D. Karlsson, R. van Leeuwen, and G. Stefanucci, *Physical Review B* **105**, 125134 (2022).
- [37] M. Schüler, M. Eckstein, and P. Werner, *Phys. Rev. B* **97**, 245129 (2018).
- [38] C. Stahl, N. Dasari, J. Li, A. Picano, P. Werner, and M. Eckstein, *Physical Review B* **105**, 115146 (2022).
- [39] J. Kaye and D. Golež, *SciPost Phys.* **10**, 091 (2021).
- [40] J. Yin, Y. hao Chan, F. H. da Jornada, D. Y. Qiu, S. G. Louie, and C. Yang, *J. Comput. Sci.* **64**, 101843 (2022).
- [41] C. C. Reeves, J. Yin, Y. Zhu, K. Z. Ibrahim, C. Yang, and V. c. v. Vlček, *Phys. Rev. B* **107**, 075107 (2023).
- [42] H. Shinaoka, M. Wallerberger, Y. Murakami, K. Nogaki, R. Sakurai, P. Werner, and A. Kauch, *Phys. Rev. X* **13**, 021015 (2023).
- [43] M. Murray, H. Shinaoka, and P. Werner, arXiv preprint arXiv:2312.03809 (2023).
- [44] F. Meirinhos, M. Kajan, J. Kroha, and T. Bode, *SciPost Phys. Core* **5**, 030 (2022).
- [45] R. van Leeuwen and N. E. Dahlen, An introduction to nonequilibrium green functions (2006).
- [46] X. Dong, E. Gull, and H. U. R. Strand, *Phys. Rev. B* **106**, 125153 (2022).
- [47] A. A. Rusakov and D. Zgid, *The Journal of Chemical Physics* **144**, 054106

- (2016), [https://pubs.aip.org/aip/jcp/article-pdf/doi/10.1063/1.4940900/14800495/054106.1\\_online.pdf](https://pubs.aip.org/aip/jcp/article-pdf/doi/10.1063/1.4940900/14800495/054106.1_online.pdf).
- [48] N. Tsuji, M. Eckstein, and P. Werner, *Phys. Rev. Lett.* **110**, 136404 (2013).
- [49] P. Werner, N. Tsuji, and M. Eckstein, *Phys. Rev. B* **86**, 205101 (2012).
- [50] R. Shimano and N. Tsuji, *Annual Review of Condensed Matter Physics* **11**, 103 (2020), <https://doi.org/10.1146/annurev-conmatphys-031119-050813>.
- [51] D. Golež, P. Werner, and M. Eckstein, *Phys. Rev. B* **94**, 035121 (2016).
- [52] A. Picano and M. Eckstein, *Phys. Rev. B* **103**, 165118 (2021).
- [53] Y. Murakami, P. Werner, N. Tsuji, and H. Aoki, *Phys. Rev. B* **94**, 115126 (2016).
- [54] T. Hong, M. Matsumoto, Y. Qiu, W. Chen, T. R. Gentile, S. Watson, F. F. Awzadi, M. M. Turnbull, S. E. Dissanayake, H. Agrawal, *et al.*, *Nature Physics* **13**, 638 (2017).
- [55] J. Demsar, K. Biljaković, and D. Mihailovic, *Phys. Rev. Lett.* **83**, 800 (1999).
- [56] R. Yusupov, T. Mertelj, V. V. Kabanov, S. Brazovskii, P. Kusar, J.-H. Chu, I. R. Fisher, and D. Mihailovic, *Nature Physics* **6**, 681 (2010).
- [57] Z. Lenarčič, D. Golež, J. Bonča, and P. Prelovšek, *Phys. Rev. B* **89**, 125123 (2014).
- [58] C. Shao, T. Tohyama, H.-G. Luo, and H. Lu, *Phys. Rev. B* **93**, 195144 (2016).
- [59] M. Eckstein and M. Kollar, *Phys. Rev. B* **78**, 205119 (2008).
- [60] Y. Murakami, P. Werner, N. Tsuji, and H. Aoki, *Phys. Rev. B* **93**, 094509 (2016).
- [61] D. Golež, Z. Sun, Y. Murakami, A. Georges, and A. J. Millis, *Phys. Rev. Lett.* **125**, 257601 (2020).
- [62] E. Wang, J. Adelinia, M. Chavez-Cervantes, T. Matsuyama, M. Fechner, M. Buzzi, G. Meier, and A. Cavalleri, *Nature Communications* **14**, 7233 (2023).
- [63] J. W. McIver, B. Schulte, F.-U. Stein, T. Matsuyama, G. Jotzu, G. Meier, and A. Cavalleri, *Nature Physics* **16**, 38 (2020).
- [64] R. Venturini, A. Mraz, I. Vaskivskiy, Y. Vaskivskiy, D. Svetin, T. Mertelj, L. Pavlovič, J. Cheng, G. Chen, P. Amarasinghe, *et al.*, *Applied Physics Letters* **120** (2022).
- [65] C. Stahl and M. Eckstein, *Phys. Rev. B* **103**, 035116 (2021).
- [66] Z. Sun and A. J. Millis, *Phys. Rev. X* **10**, 021028 (2020).
- [67] A. Zong, A. Kogar, Y.-Q. Bie, T. Rohwer, C. Lee, E. Baldini, E. Ergeçen, M. B. Yilmaz, B. Freelon, E. J. Sie, H. Zhou, J. Straquadine, P. Walmsley, P. E. Dolgirev, A. V. Rozhkov, I. R. Fisher, P. Jarillo-Herrero, B. V. Fine, and N. Gedik, *Nature Physics* **15**, 27 (2019).
- [68] K. Nasu, *Photoinduced Phase Transitions* (WORLD SCIENTIFIC, 2004).
- [69] Y. Murakami, D. Golež, M. Eckstein, and P. Werner, Photo-induced nonequilibrium states in mott insulators (2023), [arXiv:2310.05201 \[cond-mat.str-el\]](https://arxiv.org/abs/2310.05201).
- [70] A. de la Torre, D. M. Kennes, M. Claassen, S. Gerber, J. W. McIver, and M. A. Sentef, *Rev. Mod. Phys.* **93**, 041002 (2021).
- [71] C. Giannetti, M. Capone, D. Fausti, M. Fabrizio, F. Parmigiani, and D. Mihailovic, *Advances in Physics* **65**, 58 (2016), <https://doi.org/10.1080/00018732.2016.1194044>.
- [72] J. Kaye, K. Chen, and O. Parcollet, *Phys. Rev. B* **105**, 235115 (2022).
- [73] J. Kaye, K. Chen, and H. U. R. Strand, *Comput. Phys. Commun.* **280**, 108458 (2022).
- [74] J. Kaye and H. U. R. Strand, *Adv. Comput. Math.* **49**, 10.1007/s10444-023-10067-7 (2023).

### Implementation details

The attractive Hubbard Hamiltonian in Eq. (1) can be rewritten as

$$H = -t_0 \sum_{\langle j,k \rangle \sigma} \sigma e^{iqA(t)\sigma} \psi_{j\sigma}^\dagger \psi_{k\sigma} \quad (3)$$

$$+ U \sum_i \psi_{i\downarrow}^\dagger \psi_{i\downarrow} \psi_{i\uparrow}^\dagger \psi_{i\uparrow} - \frac{U}{2} \sum_{i\sigma} \psi_{i\sigma}^\dagger \psi_{i\sigma},$$

where we have used the Nambu spinors

$$\psi_i = \begin{pmatrix} d_{i\uparrow} \\ d_{i\downarrow} \end{pmatrix}. \quad (4)$$

We again use the Nambu spinors to define the anomalous Green's function

$$G(t, t') = \langle \psi(t) \psi^\dagger(t') \rangle = \begin{pmatrix} \langle d_\uparrow d_\uparrow^\dagger \rangle(t, t') & \langle d_\uparrow d_\downarrow \rangle(t, t') \\ \langle d_\downarrow d_\uparrow^\dagger \rangle(t, t') & \langle d_\downarrow d_\downarrow \rangle(t, t') \end{pmatrix}, \quad (5)$$

which is the quantity we compute by solving the KBE.

We solve this system within the DMFT approximation on a Bethe lattice, giving the hybridization function

$$\Delta(t, t') = \Delta_R(t, t') + \Delta_L(t, t') \quad (6)$$

$$\Delta_R(t, t') = \frac{1}{2} \bar{t}_0(t) \sigma_z G(t, t') \sigma_z \bar{t}_0^*(t') \quad (7)$$

$$\Delta_L(t, t') = \frac{1}{2} \bar{t}_0^*(t) \sigma_z G(t, t') \sigma_z \bar{t}_0(t'), \quad (8)$$

with hopping matrix elements given by

$$\bar{t}_0 = \begin{pmatrix} e^{i\phi(t)} & 0 \\ 0 & e^{-i\phi(t)} \end{pmatrix}, \quad (9)$$

$$\phi(t) = \int_0^t E(s) ds \quad (10)$$

due to the Peierls substitution.

The impurity problem is solved using the fully self-consistent second Born approximation. In this approximation, the Fock term is given by

$$\Sigma_{ij}^F(t) = iU(t) G_{ij}^<(t, t^-) \delta_{i\bar{j}}, \quad (11)$$

and the Hartree term cancels the chemical potential since we are at half-filling. There are two second-order diagrams:

$$\Sigma_{ij}^B(t, t') = U(t) U(t') G_{ij}(t, t') G_{i\bar{j}}^>(t, t') G_{ij}(t', t), \quad (12)$$

$$\Sigma_{ij}^E(t, t') = -U(t) U(t') G_{i\bar{j}}^>(t, t') G_{i\bar{j}}^>(t, t') G_{i\bar{j}}^>(t', t). \quad (13)$$

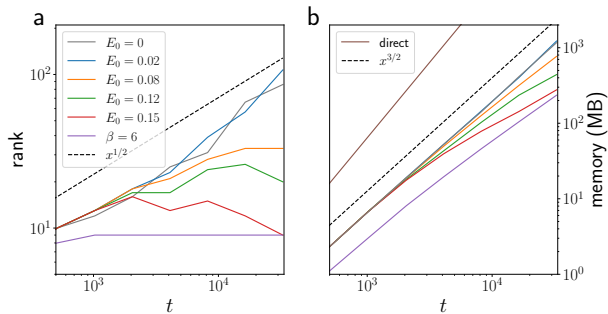


FIG. 5. (a) Rank of the truncated SVD of the largest block in a HODLR decomposition of Green's function at timestep  $T$ . Results for several different pump strengths are presented.  $\beta = 6$  is a result in the equilibrium disordered state. (b) Total memory required to store Green's function and self-energy for the presented pump strengths.

The hybridization  $\Delta[G](t, t')$  and the self-energy  $\Sigma[G](t, t')$  depend on the Green's function, and we maintain self-consistency using fixed-point iteration terminating when the maximum difference of the Green's function at subsequent iterates is less than  $10^{-10}$ .

We use the fifth-order backward differentiation formula multistep method to discretize the KBE. Gregory quadrature is used to discretize memory integrals to fifth-order accuracy. The discrete Lehmann representation [72], implemented in `libdlr` [73], is used to discretize the imaginary time variables appearing in the vertical leg of the Keldysh contour, as in Ref. [74]. We have confirmed that the compression of the Green's function using the HODLR scheme preserves conservation laws, namely the density and energy, to within the SVD truncation tolerance used in the scheme, which we set to  $10^{-8}$ .

In the pump-probe experiments, we measure the current, given by

$$j(t) = \text{Im}(\text{Tr}[\sigma_z(\Gamma_L(t) - \Gamma_R(t))]) \quad (14)$$

$$\Gamma_{R/L}(t) = -i[G * \Delta_{L/R}]^<(t, t), \quad (15)$$

with  $*$  the convolution operator on the three-legged Keldysh contour.

### Numerical ranks in HODLR scheme

Our time propagation scheme compresses the Green's function using a HODLR decomposition [39]. A truncated SVD is performed on each block of the decomposition, and updated on-the-fly, with singular values below  $10^{-10}$  discarded. The numerical ranks of these blocks (within this precision) determine the compressibility of the Green's functions, and the performance of the scheme.

Fig. 5(a) shows the growth of the maximum block rank  $k$  with the number of time steps. At inverse temperature  $\beta = 6$ , the system is in a disordered state, and the Green's functions decay exponentially on their off-diagonal. This leads to a rapid saturation of the ranks, giving an  $\mathcal{O}(N^2 \log N)$  computational complexity of the algorithm, and an  $\mathcal{O}(N \log N)$  memory complexity, with  $N$  the number of time steps. The behavior is similar for the simulations in which a low-temperature state is excited with a strong pump (i.e.  $E_0 = 0.15$ ), destroying the superconducting state. At low temperature, in the ordered state, although the blocks are still numerically low rank with  $k \ll N$ , they grow as  $k \propto \sqrt{N}$ , leading to an  $\mathcal{O}(N^3 \log N)$  computational complexity and  $\mathcal{O}(N^{3/2} \log N)$  memory complexity. Nevertheless, while the memory usage, shown in Fig. 5(b), reflects the expected scaling, the wall clock time shown in Fig. 4 reflects approximately  $\mathcal{O}(N^2)$  scaling, suggesting that lower-scaling steps of the algorithm dominate throughout the time scale of this simulation.